Available online at www.sciencedirect.com
ScienceDirect
Journal of Sound and Vibration 299 (2007) 83–98
JOURNAL OF SOUND AND VIBRATION
www.elsevier.com/locate/jsvi

Experimental modal testing using pressurized air excitation

S. Vanlanduit*, F. Daerden, P. Guillaume

Department of Mechanical Engineering (MECH), Vrije Universiteit Brussel, Pleinlaan 2, B-1050 Brussels, Belgium

Received 6 October 2005; received in revised form 30 March 2006; accepted 27 June 2006
Available online 11 September 2006

Abstract

Non-fixed excitation methods are often needed in modal analysis (for instance in quality control applications). Several non-fixed methods exist to perform this task: impact hammer, electro-magnetic, acoustic and laser excitation. In this article the use of pneumatic excitation using an impinging air jet is proposed as an alternative. Through a detailed experimental study it is shown that forces up to 0.6 N can be attained, while with the current valve technology one can excite up to 1 kHz. Two application cases are considered: a modal analysis of a cantilevered beam and a vibration test of a hard disk.

1. Introduction

In experimental modal analysis the structure under test is excited while both the perturbation force and the vibration response are measured [1]. The most common technique to stimulate the structural vibration is by using an electrodynamic shaker. However, it is well known that connecting a shaker to the structure alters the structure's dynamics. Moreover, due to the impedance mismatch between the structure and the shaker, the force tends to drop at resonance frequencies leading to poor signal-to-noise ratio in the neighborhood of these frequencies [2]. The impact hammer test method is a non-fixed technique that does not have these disadvantages. On the other hand, using a hammer has other important restrictions: the method required user interaction since mostly a manual hammering method is applied. In addition, during a short-time interval mechanical contact between the structure and the hammer is made, which makes the method difficult to apply to light and brittle objects. Other non-contacting methods—as for instance acoustic, magnetic and laser stimulation—exist as alternatives. Unfortunately, these techniques are either limited to high frequencies and low force levels (acoustic and laser excitation [3]) or cannot be used on non-metallic structures (magnetic excitation [4]). In addition, with these non-contact stimulation methods it is very difficult to obtain a measurement of the excitation force, and therefore the determination of a scaled modal model is cumbersome [5].

Previous results have shown that pneumatic excitation using pressurized air can be used to excite a structure [6]. In this article, an extensive experimental validation of the use of pressurized air excitation in modal analysis will be reported. It will be shown that pneumatic excitation is an attractive alternative that provides perturbation forces up to 0.6 N at frequencies up to 1 kHz. Firstly, the working principle of pneumatic

*Corresponding author. Tel.: +32 2 629 2805; fax: +32 2 629 2865.
E-mail address: steve.vanlanduit@vub.ac.be (S. Vanlanduit).

0022-460X/$ - see front matter © 2006 Elsevier Ltd. All rights reserved.
doi:10.1016/j.jsv.2006.06.052

excitation is described in Section 2. Then, a detailed experimental study of the force signals obtained using pneumatic excitation is performed in Section 3. Also, the parameters that affect the magnitude and frequency spectrum of these force signals are investigated. The next two sections present different application cases: the modal analysis of a cantilever beam (Section 4) and vibration analysis of a hard disk drive (Section 5). Finally, conclusions are drawn in Section 6.

2. Pneumatic excitation

2.1. Introduction

The impingement of a jet on a structure results in a force F that is exerted. The magnitude of this force is determined by the change of momentum of the jet

$$F = \dot{m} C_m \tag{1}$$

with $\dot{m}$ the mass flow (in kg/s) and C_m the mean gas flow velocity [7].

2.2. Valve characteristics

When using a valve to control the air flow, the mass flow $\dot{m}$ can be approximated by [8]

$$\dot{m} = C P_u \rho_0 \sqrt{\frac{293}{T_u}} \sqrt{1 - \left(\frac{P_d/P_u - b}{1-b}\right)^2} \quad \text{if } P_d/P_u \geqslant b \tag{2}$$

and

$$\dot{m} = C P_u \rho_0 \sqrt{\frac{293}{T_u}} \quad \text{if } P_d/P_u < b \tag{3}$$

with P_d and P_u the downstream and upstream absolute pressures, T_u the upstream temperature (in degrees Kelvin), ρ_0 the ambient air density, b the critical pressure ratio and C the specific mass flow (expressed in $m^3/(s\,Pa)$). It is clear from Eqs. (2) and (3) that the measurement of the pressures directly results in the mass flow (assuming that C—which is a valve characteristic—is known). Because the gas flow velocity (in Eq. (1)) is also proportional to the upstream pressure (by Bernouilli's law) the exerted force is proportional to the upstream pressure (all other quantities determining the force are constants).

One possibility is the use of servo-valves which can be opened and closed in a continuous manner. Since the mass flow is dependent on the opening of the valve this means that an arbitrary continuous excitation force can be exerted using a servo-valve. Unfortunately, servo-valves can only excite up to frequencies of about 100 Hz.

On-off valves, on the other hand, can provide a discontinuous excitation with opening–closing times up to 1 ms. The most straightforward choice of drive signal is a pulse signal that opens the valve during a time T_p (i.e. the pulse width of the signal) and then closes the valve for the rest of the measurement period T (with $T \gg T_p$). In this article the Matrix 821 KK series valve is used (the characteristics of the valve can be found in Table 1). At the end of the valve a nozzle is mounted. This results in the outlet flow to be less turbulent than the interior flow in the nozzle.

3. Force measurement experiments

In order to determine the exerted force of a pneumatic excitation system, the impinging jet was aimed at a disk that was mounted on a Type 8001 Bruel&Kjaer Impedance head (see Fig. 1). The upstream pressure was measured using a Data Instruments Type XCA5-60GN pressure gauge. The measured gauge pressure P_m is the upstream pressure relative to the ambient pressure $P_0 : P_m = P_u - P_0$. As will be shown in the experimental result that follow in this section, the pressure P allows to determine the exerted force.

Table 1
Valve characteristics of the matrix valve

Characteristic	Value	Units
Producer	Matrix S.p.A. Italie	—
Identification code	OX 821.104C2KK	—
Dimensions	$12 \times 37 \times 28.5$	mm
Mass	25	g
Supply voltage	5	V(dc)
Speed-up in tension	24	V(dc)
Nominal electric power	0,8	W
Response time in opening	<1	ms
Response time in closing	<1	ms
Maximum frequency	500	Hz
Product life expectancy	>500	Million cycles
Critical pressure ratio b	0,433	—
Specific mass flow C	4.3e7	$m^3/(s \times Pa)$
Maximum flow	3e-3	m^3/s
Operating pressure	$0 \rightarrow 6000$	Pa

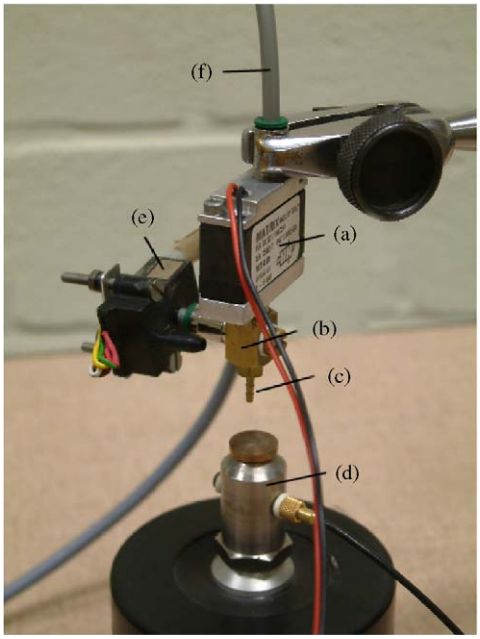

Fig. 1. Setup of the pressurized air force measurement experiment: (a) valve, (b) output manifold, (c) nozzle, (d) force sensor, (e) pressure sensor, (f) supply.

Firstly, the influence of the supply pressure on the resulting impact force on the disk was measured. In this case a pulse with a pulse width of 2 ms was used as the valve control signal. As an example the time history of the 2 ms pulse force with a supply pressure of 4 bar is shown in Fig. 2. The relation between the supply pressure and the force level is shown by plotting the peak value versus the supply pressure (see Fig. 3). It appears from the results in Fig. 3 that there is a linear relation between the supply pressure and the maximum of the measured (pulse-shaped) force (the correlation coefficient of the data in Fig. 3 is 99.9%). The linear dependency of the force F on the upstream pressure P_u is also apparent from Eq. (1) up to Eq. (3).

A second important consideration is the relation of the force magnitude in function of the distance of the nozzle to the disk. Therefore, consecutive experiments were performed (with a 2 ms pulse and 3 bar supply

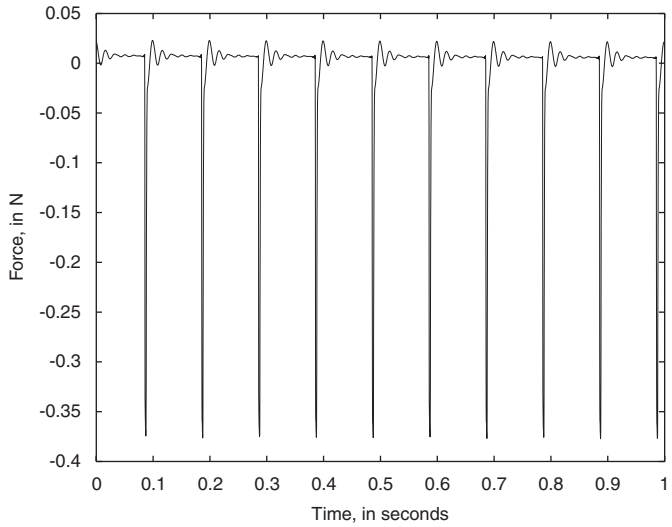

Fig. 2. Time history of the measured impulse force signals.

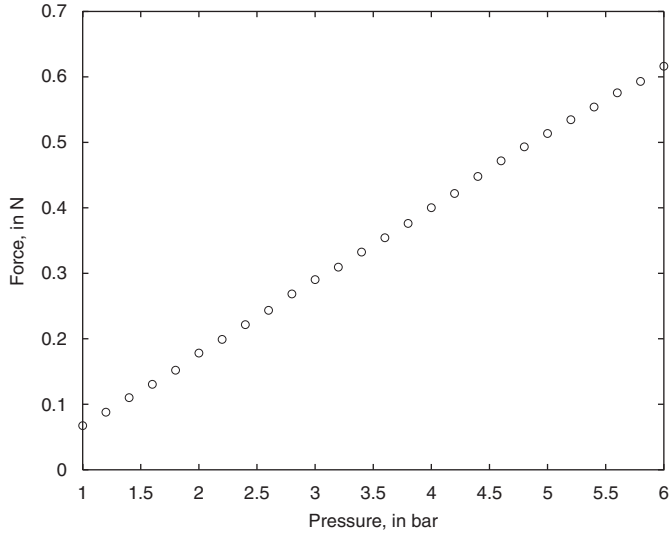

Fig. 3. Force exerted by the pressurized air excitation in function of the input gauge pressure P_m.

pressure) altering this distance between 1 and 40 mm with a resolution of 1 mm. The graph in Fig. 4 shows that the influence in negligible for distance up to 20 mm, while even for larger distances only 15% reduction in force is obtained. This is in agreement with the division between the so-called near-field region and the far-field region that is reported in literature [9]. In the latter region, the fluid has experienced turbulent mixing with the quiescent fluid.

The valve opening and closing times determine the frequency range that can be covered using pneumatic excitation. According to the specifications of the Matrix valve (see Table 1) opening closing frequencies up to 1 ms can be obtained. This was experimentally verified by generating pulses with a duration varying from 0.5 up to 4 ms in 0.1 ms steps (the supply pressure was 3 bar). It appeared that from 0.8 ms on there was a monotone increasing trend of the force level with increasing pulse widths (see Fig. 5). For values smaller than 0.8 ms the force was significantly smaller. It is important to remark that this threshold (the value of 0.8 ms where a discontinuity in the applied force occurs) is dependent on the supply pressure. Indeed, it was observed

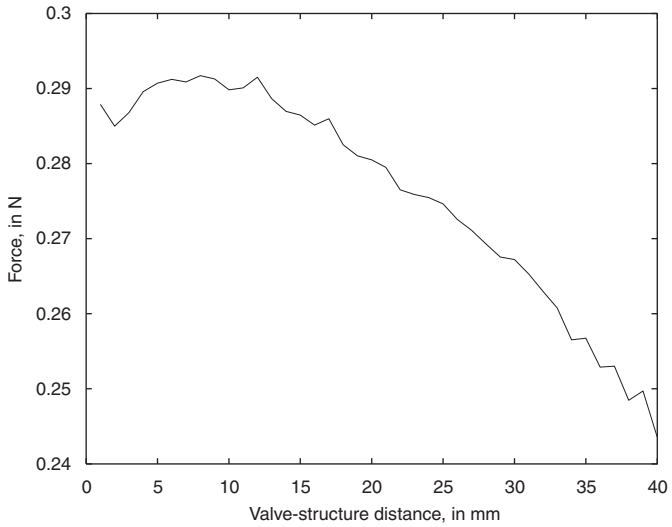

Fig. 4. Force exerted by the pressurized air excitation in function of the distance of the nozzle from the structure.

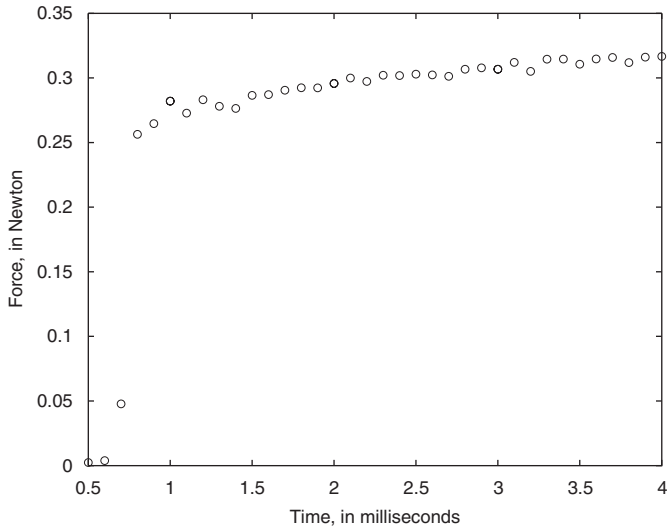

Fig. 5. Exerted force of the pressurized air jet in function of the pulse width.

that for smaller pressures shorter switching times could be realized. This means that in order to excite medium and high frequencies not only the pulse width but also the supply pressure has to be reduced. In Fig. 6 a selection of the force spectra agreeing to measurements performed with pulses with different widths are shown. The spectra shown in this figure are obtained by applying an FFT to ten periods of a pulse train (the repetition rate of the pulse train was 10 Hz). Because in this case the energy of the excitation signal (pulse train) is concentrated at FFT lines $10.k$, with $k = 1, 2, \ldots$ the lines that are not a multiple of 10 are not shown in Fig. 6 (and also in the spectra following in the remaining of the paper). The amplitude spectra in Fig. 6 are shown in dB with a 0 dB reference value of 1 N. The forces pertaining to the two smallest pulse widths (0.5 and 0.6 ms) are unacceptably low with measurement levels close to the noise level (amplitude values below 120 db which equals 1 μm). The 0.7 ms signal (see '*' signs in Fig. 6) has a fairly flat spectrum up to 1800 Hz with a reasonable amplitude level around −90 dB (or 30 μm). The two largest pulse durations provide a much higher amplitude level but their spectra show notches in the depicted frequency range. In fact, the spectrum of the

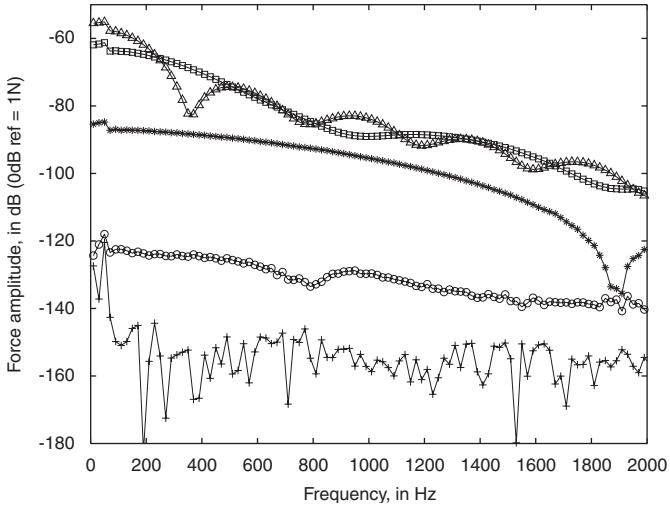

Fig. 6. Force amplitude spectrum in dB in function of the pulse width: $+$, 0.0005 s; $\bigcirc$, 0.0006 s; $*$, 0.0007 s; $\square$, 0.001 s and $\triangle$, 0.002.

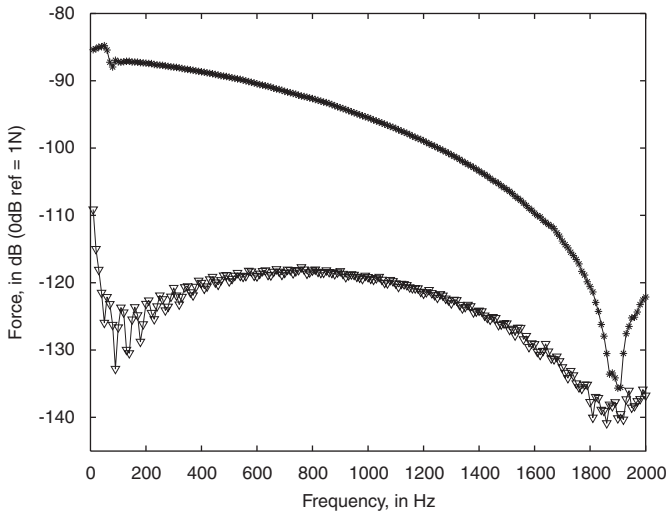

Fig. 7. Force amplitude spectrum of the 0.001 s pulse and standard deviation of the pulses spectrum computed from 100 measurements.

excitation pulse has a notch at multiples of $f_0 = 1/T_p$ with T_p the pulse duration. However, because of deviations between the opening and closing times the actual pulse duration differs from the pulse duration of the electronically generated signal. The repeatability of the excitation is illustrated in Fig. 7. It can be seen from this figure that the standard deviation of the spectrum is about 30 dB lower than the signal level for frequencies up to 1000 Hz. For higher frequencies this ratio decreases because the excitation level decreases.

By measuring in the experimental setup described in this section the pressure P_m at the outlet of the valve together with the force F measured by the transducer, a calibration curve C can be calculated

$$C(f) = \frac{\mathscr{F}F(f)}{\mathscr{F}P_m(f)}, \tag{4}$$

where $\mathscr{F}$ denotes the discrete Fourier transform of the respective time domain signals F and P_m. It is important to remark that Eq. (4) can only be used because the excitation is periodic (i.e. a periodic pulse train

signal). For non-periodic (stochastic) excitation signals the so-called H_1 estimator—that is defined by the ratio between the cross-power spectrum divided by the auto-power spectrum—is preferred. During a modal analysis the pressure measurements together with the calibration curve can be used to obtain the force levels (which cannot be measured directly). This calibration procedure will be validated in the following section.

In Figs. 8 and 10 the influence of the pulse width and the supply pressure on the calibration curves is given. For pulse widths up to 0.7 ms, it can be seen in Figs. 8 and 10 that the actual pressure P_m is below the noise level on the pressure measurement and consequently the calibration curves are biased towards a lower value. The calibration curves in Fig. 10 corresponding to the two largest pulse widths (1 and 2 ms) on the other hand, correspond very well. With respect to the supply pressure there is a good agreement between the different calibration curves (see Fig. 10) in the frequency range up to 1500 Hz (except for the 1 bar curve that has again a pressure measurement below the noise level). One indication of the quality of the calibration is the so-called

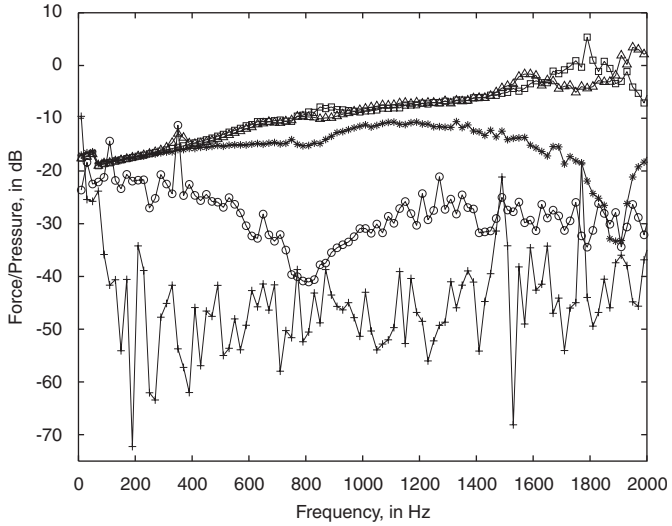

Fig. 8. Calibration curves in function of the pulse width: +, 0.0005 s; ○, 0.0006 s; ∗, 0.0007 s; □, 0.001 s and △, 0.002.

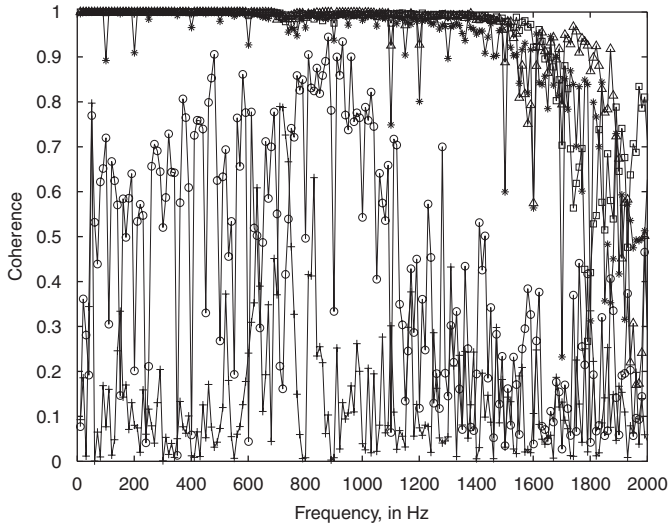

Fig. 9. Coherence function of the calibration curves in function of the pulse width: +, 0.0005 s; ○, 0.0006 s; ∗, 0.0007 s; □, 0.001 s and △, 0.002.

coherence function:

$$\mathrm{Coh}(f) = \frac{|G_{FP_m}(f)|^2}{G_{FF}(f)G_{P_mP_m}(f)}, \tag{5}$$

where G_{XY} and G_{XX} denote the cross- and autopower spectra. In Figs. 9 and 11 the coherence function of the calibration curves shown in Figs. 8 and 10 is given. For the varying pulse widths the two shortest pulses give rise to an unacceptably low coherence, while all other pulses result in coherence values above 0.9 (at least in the frequency band up to 1500 Hz). The coherence of the varying supply pressures calibration is good (>0.9) for all pressures for frequencies up to 1500 (except for the 1 bar curve that has lower coherence at isolated frequency lines below 1500 Hz) (see Figs. 8–11).

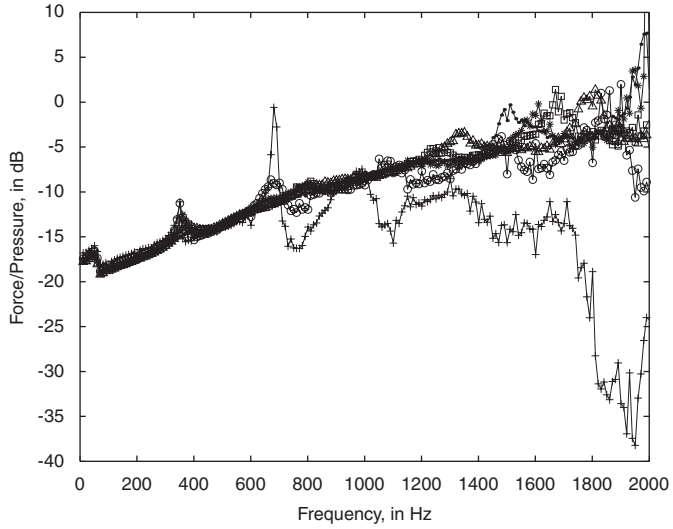

Fig. 10. Calibration curves in function of the input pressure: +, 1 bar; ○, 2 bar; ∗, 3 bar; □, 4 bar; △, 5 bar and ·, 6 bar.

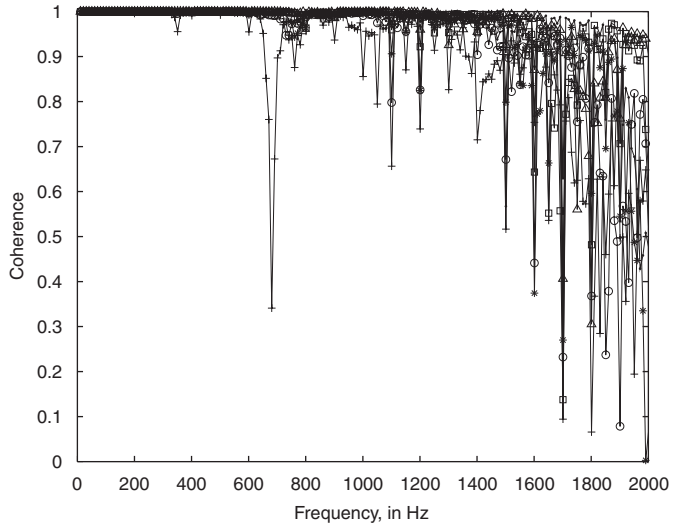

Fig. 11. Coherence function of the calibration curves in function of the input pressure: +, 1 bar; ○, 2 bar; ∗, 3 bar; □, 4 bar; △, 5 bar and ·, 6 bar.

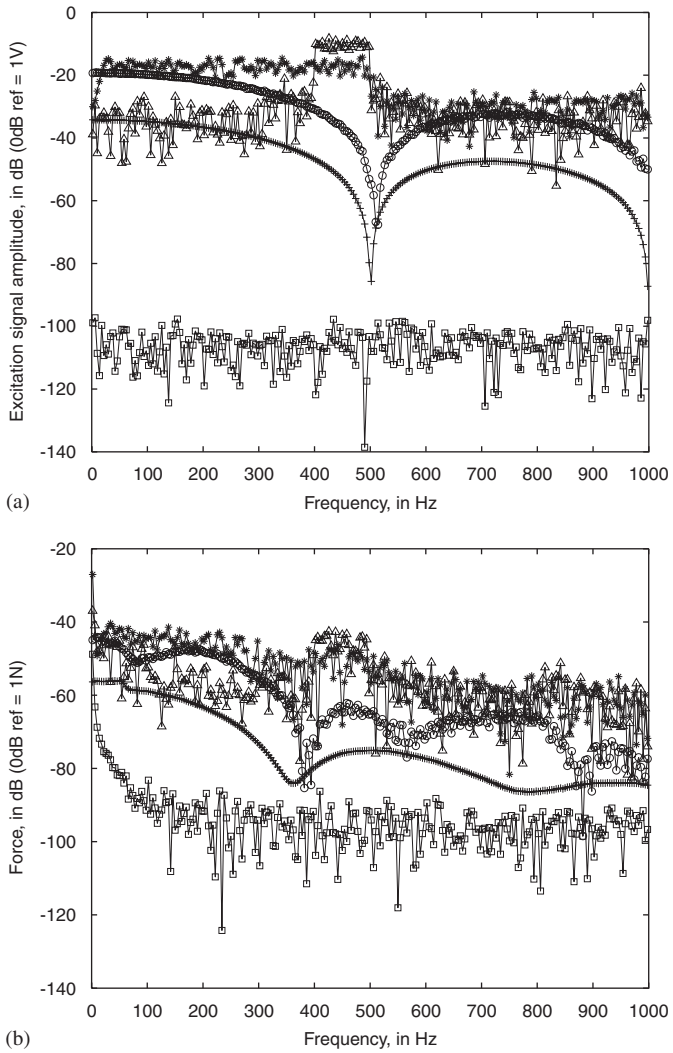

Fig. 12. Amplitude spectrum for different excitation signals: generator signal (left) and measured force signal (right). +, pulse, 2 ms, ◯, maximum length binary sequence (MLBS), ∗, square wave sweep from 10 up to 500 Hz, □, force with valve always open and △, multi-frequency binary sequence (MFBS).

Besides the use of a pulse excitation different alternative binary signals exist to stimulate the structure under test. The maximum length binary sequence (MLBS) [10] is a signal with an autocorrelation function that approximates the autocorrelation of Gaussian noise excitation (i.e. a dirac pulse). The major disadvantage of the MLBS signal is that it does not allow the construction of an excitation signal with an arbitrary amplitude spectrum (for instance the excitation of a certain frequency band). Using a square wave with a sweep of the frequency between two predefined frequencies the energy can be concentrated in the band of interest. However, it is not possible to change the levels of the amplitude spectrum (e.g. an increasing amplitude for increasing frequencies). The so-called multi-frequency binary sequence (MFBS) [10] can be used when an arbitrary amplitude spectrum is required. The amplitude spectra of the excitation signals and the measured forces of the aforementioned signals are given in Fig. 12. From this figure it is clear that the different binary sequences have amplitude levels that are up to 20 dB larger than the pulse excitation. In contrast to the binary sequences, the pulse excitation results in a much smoother amplitude spectrum (the distortions in the binary sequence spectra are caused among other things by the asymmetrical valve operation). Therefore pulse signals will be used in the remaining of this article.

4. Cantilevered beam experiment

In this section the use of pneumatic excitation will be validated by virtue of an experimental modal analysis of a cantilevered aluminium beam (beam dimensions: $425 \times 20 \times 2\,\text{mm}^3$). As a reference the beam is firstly excited using a mechanical impuls generated using a Bruel&Kjaer Type 4810 mini shaker. A force transducer was used to measure the applied loads (see the setup in Fig. 13). Remark that the shaker was not attached in a fixed manner to the structure in order to avoid structure–shaker interaction (the beam was excited by letting the shaker apply a hammer-like impulse to the beam). The vibration responses were measured in a grid of 210 locations (i.e. a 3×70 mesh) using a Polytec PSV 300 scanning laser Doppler vibrometer. The frequency resolution of the measurement was 1 Hz and no averages were performed (this means that the complete measurement took about 3.5 min).

Then the same experiment was repeated while replacing the shaker (and force cell) by the valve (see setup in Fig. 14). The calibration curve measured before (see Section 3) was used in order to compute: (a) the applied force and (b) the frequency response functions (FRFs) for the pressurized air experiment. The FRFs for both experiments (mechanical impact and pressurized air excitation) are shown in Fig. 15. For the calculation of the FRFs a rectangular window was applied. It is hard to distinguish the FRFs from both excitation devices in the Fig. 15. Some artifacts can be observed in Fig. 15, in particular at 350 Hz. These artifacts are torsional modes that are excited because the exciter is not located exactly in the middle of the beam. The modal parameters identified from the two sets of FRFs are in good agreement (see Table 2 for both resonance frequencies and

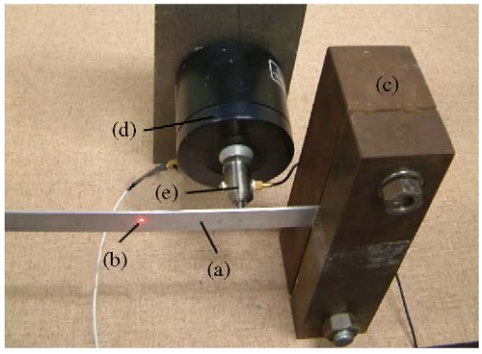

Fig. 13. Setup of the cantilever beam experiment with impact excitation. (a) aluminium beam, (b) laser Doppler vibrometer spot, (c) support, (d) shaker, (e) impedance head.

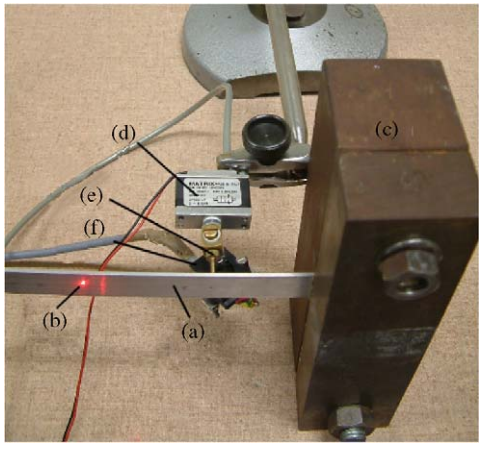

Fig. 14. Setup of the cantilever beam experiment with impact excitation. (a) aluminium beam, (b) laser Doppler vibrometer spot, (c) support, (d) valve, (e) nozzle, (f) pressure sensor.

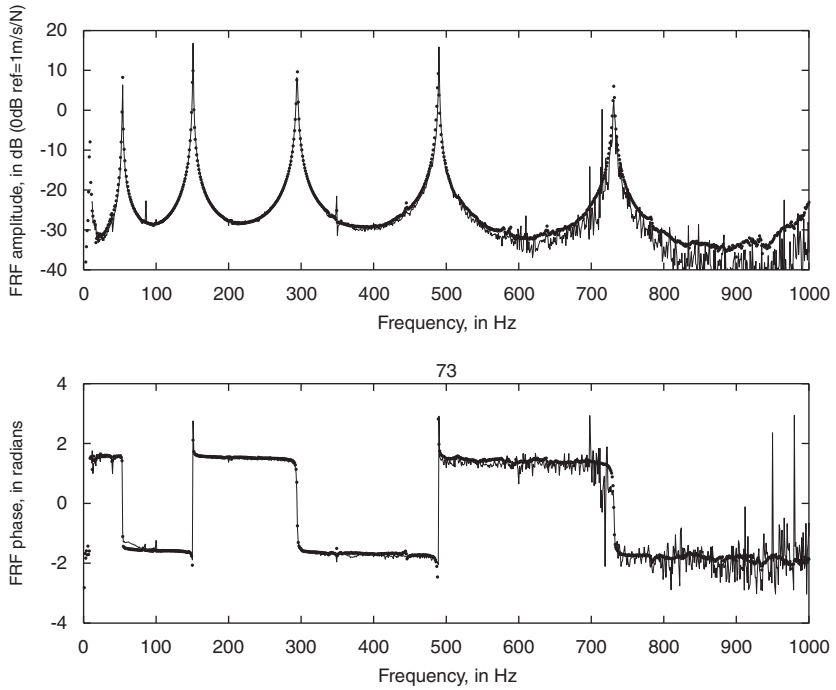

Fig. 15. Typical frequency response function (FRF) of the cantilever beam experiment: from impact measurements (dotted line) and from pressurized air experiment (full line).

Table 2
Modal parameters of the aluminium beam experiments with mechanical impact and pneumatic excitation. f_r: resonance frequencies, ξ_r: damping values in %.

Mode number	f_r impact	f_r pneumatic	dev. in %	ξ_r impulse	ξ_r pneumatic	dev. in %
1	53.8	53.8	−0.1	0.3	0.5	−82.0
2	150.6	150.8	−0.1	0.2	0.2	5.1
3	294.6	295.0	−0.2	0.2	0.2	−0.6
4	488.8	489.6	−0.2	0.2	0.2	−4.0
5	731.0	732.1	−0.2	0.1	0.2	3.8
6	1020.2	1021.2	−0.1	0.1	0.2	−85.6
7	1360.6	1361.6	−0.1	0.2	0.0	120.0

damping values, and Fig. 16 for the mode shapes). It has to be remarked that since the damping of the beam is quite low, the relative deviations are quite large for some of the modes (e.g. modes 1, 6 and 7). Furthermore, a degradation of the quality can be observed in the mode shapes in Fig. 16 at several positions. This is due to the fact that a laser Doppler vibrometer is used as a sensor (so-called speckle dropouts occur at locations with a dark speckle and give rise in a decrease of the reflected laser light).

Once the FRF $H(f)$ of the impact experiment is available, the applied force spectrum $\mathscr{F}F_p$ of the pressurized air excitation can also be computed from the velocity response spectrum $\mathscr{F}V_p$ by using the pseudoinverse $H(f)^{-1}$ of the FRF matrix [11]:

$$\mathscr{F}F_p(f) = \mathscr{F}V_p(f)H(f)^{-1}. \tag{6}$$

When these values are compared with the force estimate that is obtained from the calibration (see Fig. 17) it can be concluded that a deviation of 4.6% is present in the frequency band up to 700 Hz. It is important to

remark that the inversion procedure in Eq. (6) is poorly conditioned, resulting in erroneous results (one can for instance notice the peaks in Fig. 17 at the resonance frequencies of the structure). If the calibrated force of the aluminium beam pressurized air experiment is compared with the force of the calibration experiment (see Section 3) it can be seen that the agreement is quite good. Indeed, there is only 4.3% deviation between the force amplitude spectra that are represented in both curves in Fig. 18.

5. Disk drive experiment

This section represents the quality control application case of a disk drive. With the increasing storage density and spindle rotation speeds of disk drives the vibration of the suspension and the hard disk drive have

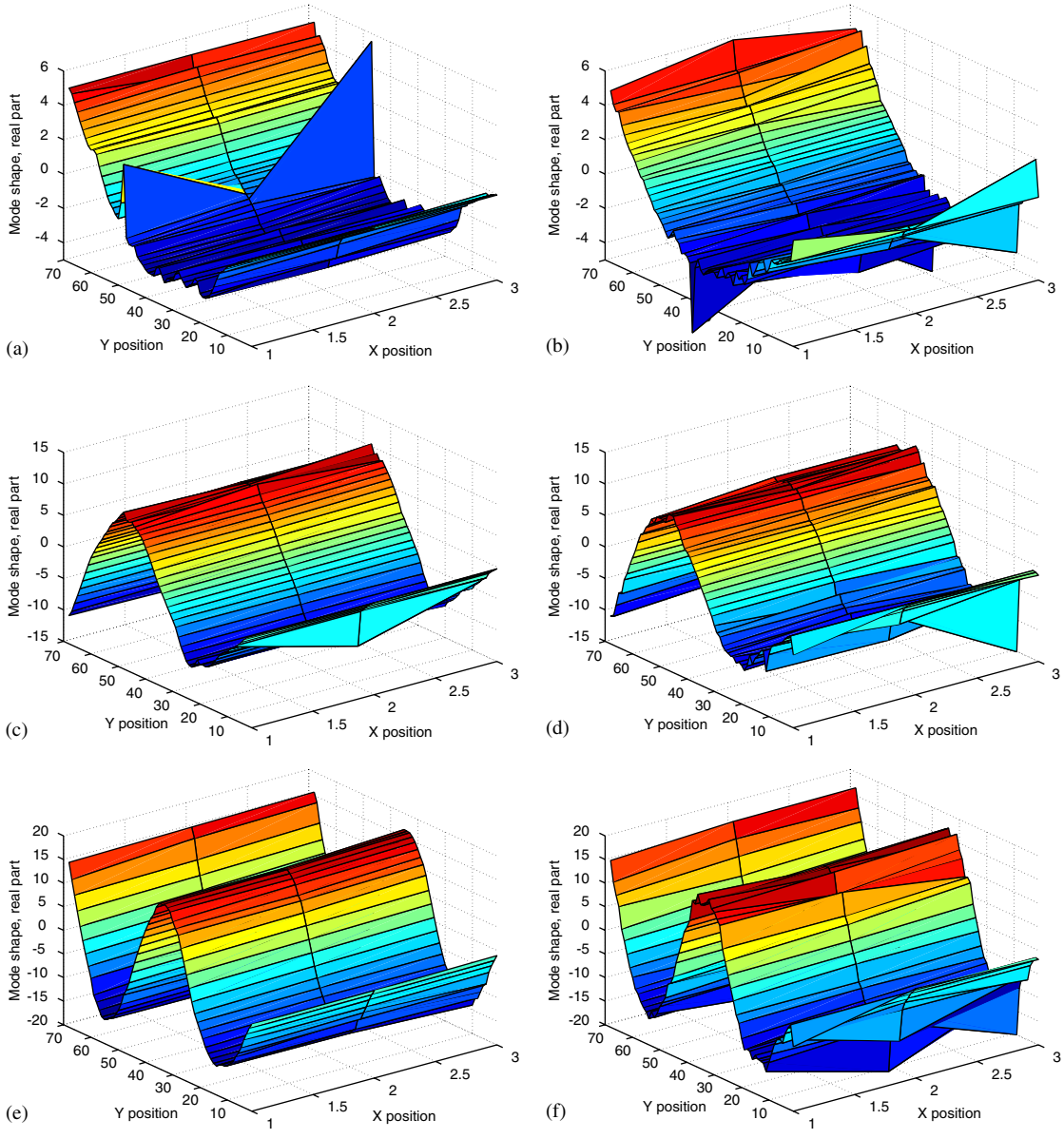

Fig. 16. First five mode shapes of the cantilevered beam: from impact experiment (left) and from pressurized air experiment (right).

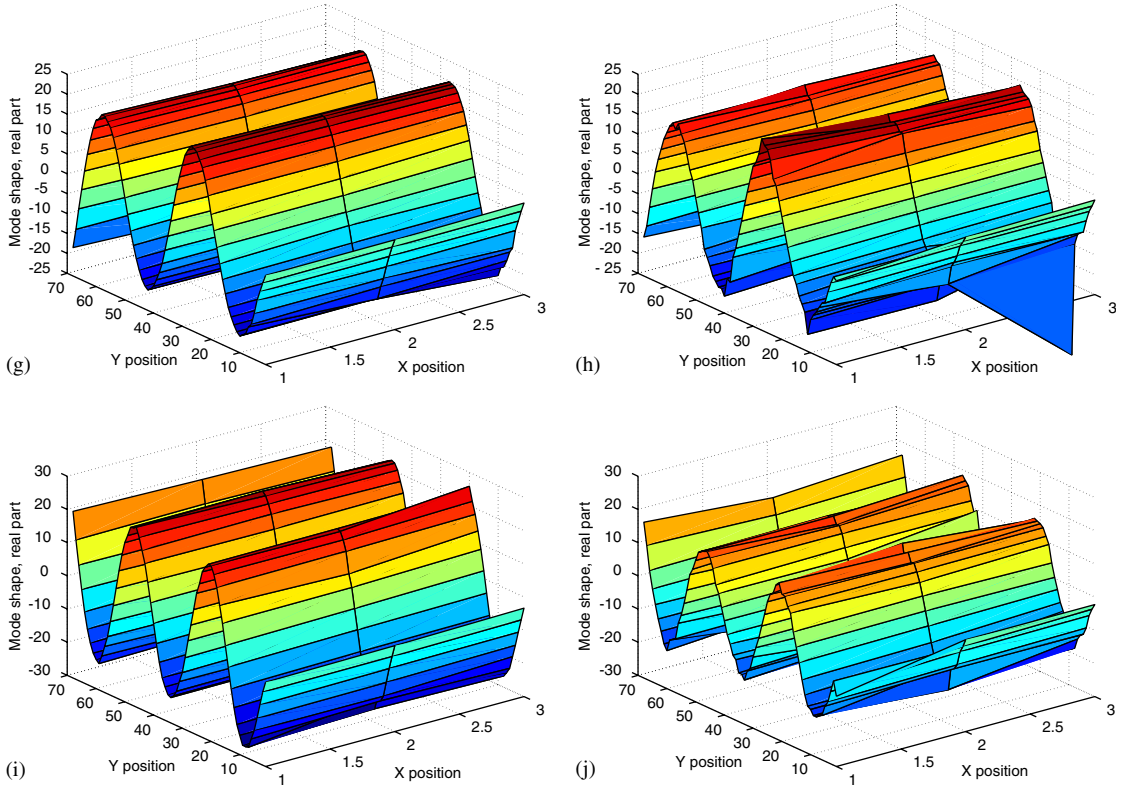

Fig. 16. (*Continued*)

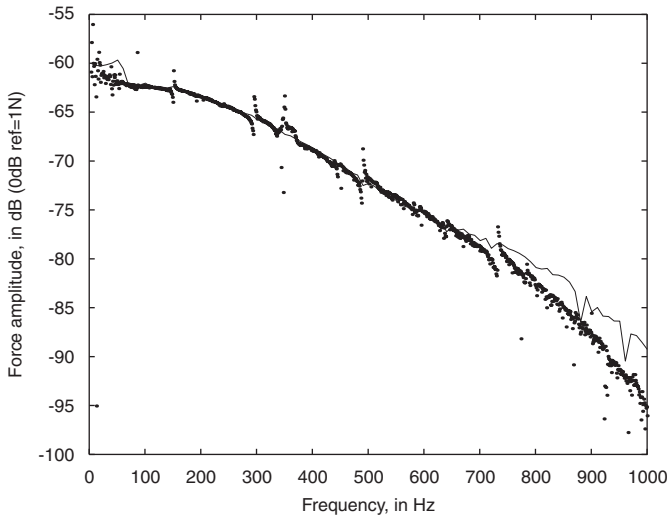

Fig. 17. Force amplitude spectrum of the cantilever beam experiment: estimated using the inverse FRF from velocities (dots) and estimated from the pressure sensor (full line).

to be controlled in order to reduce the track mis-registration. In order to control the quality of the drives in the production process it is essential that displacements of the hard disk arm when it is excited by an external force can be measured. Due to its large displacement values, the first vibration mode is of particular interest for hard disk drive manufacturers.

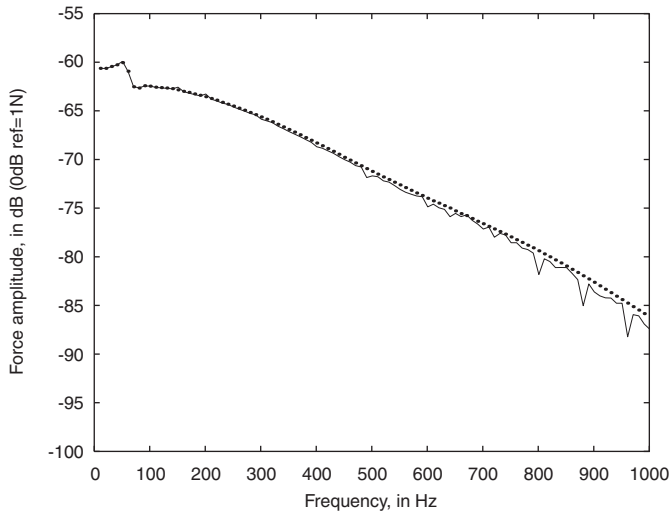

Fig. 18. Force amplitude spectrum: estimated force for the cantilevered beam (full line) and measured force on a force sensor mounted on a shaker (dotted line).

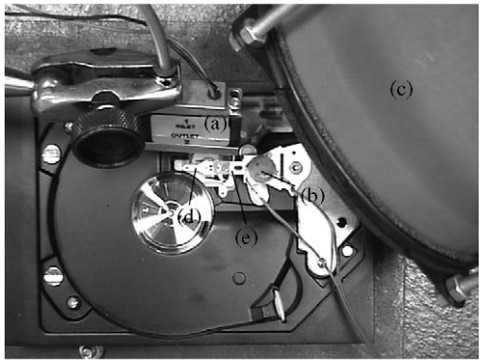

Fig. 19. Setup of the disk drive experiment. (a) valve, (b) piezo, (c) loudspeaker, (d) disk drive arm, (e) disk drive suspension.

In the experiment described in this section three different stimulation techniques are compared in view of their application to quality control (see the setup of the experiment in Fig. 19):

- a PZT actuated with a sine sweep between 0 and 4 kHz.
- a loudspeaker generating an acoustic sine sweep excitation between 0 and 4 kHz.
- a 0.4 ms pressurized air pulse with a supply pressure of 0.5 bar.

The responses of each of the test signals was measured using a Polytec scanning laser Doppler vibrometer. The average of the velocity responses is shown in Fig. 20. The magnitude of the acoustic signal is quite low and consequently the measured signal is noisy. The PZT and pressurized air velocity spectra clearly show the presence of the first vibration mode at 277.5 Hz (the peak around 20 Hz represents a rigid body mode). It can also be seen in Fig. 20 that the resonance peak of the PZT is slightly shifted due to the mass loading of the PZT on the disk drive arm. From the mode shapes in Fig. 21 it can be concluded that all three mode shapes correlate well, although the acoustic excitation mode shape is much more noisy. The availability of a non-contact excitation (as opposed to the PZT that has to be glued on the structure) is important when one wants to apply the method for in-line inspection of hard disks or other electronic products.

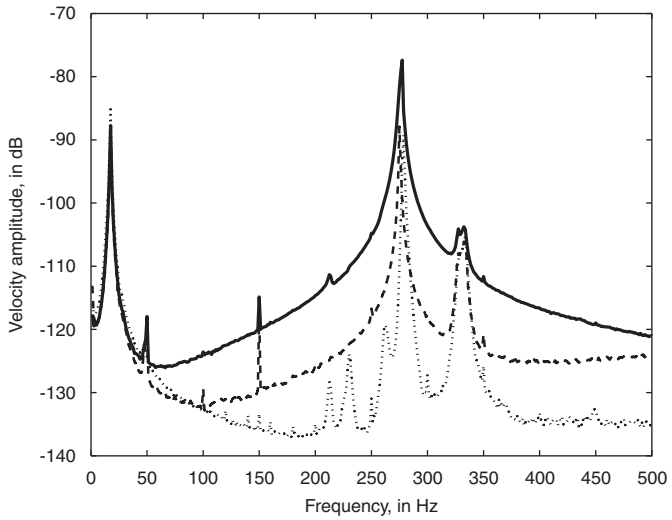

Fig. 20. Velocity amplitude spectrum of the disk drive experiment: acoustic excitation (dots), piezo excitation (dashed) and pressurized air excitation (full line).

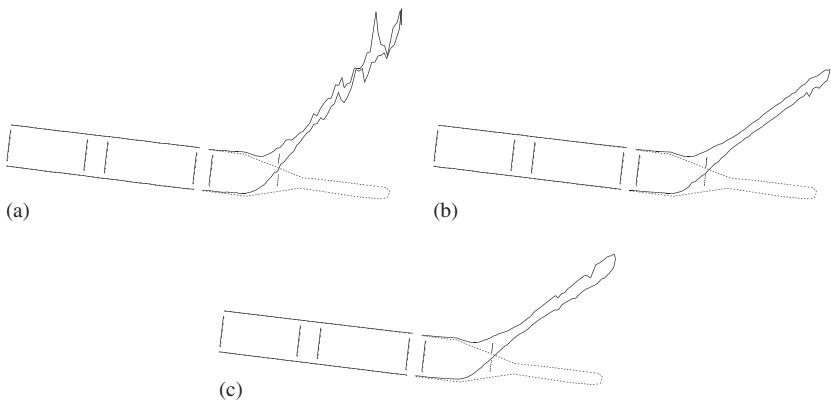

Fig. 21. Bending mode shape of the disk drive: (a) from acoustic excitation, (b) from PZT excitation and (c) pressurized air excitation. Modal assurance criterium (MAC) values: $\mathrm{MAC}((a),(b)) = 0.98$, $\mathrm{MAC}((b),(c)) = 0.99$, $\mathrm{MAC}((a),(c)) = 0.97$.

6. Conclusions

The use of pressurized air—controlled with fast on-off valves—is a cheap and flexible means to excite a structure in a modal analysis experiment. Using a calibration curve the applied force can be obtained through the measurement of the outlet pressure. Forces up to 0.6 N can be exerted. The method was successfully used to estimate vibration modes of a cantilevered beam up to 1000 Hz.

Because pressurized air is usually available in industrial environments the method could be applied for quality control of manufacturing processes (because of the magnitude of the force that can be applied mainly electronic components are within the application scope).

Acknowledgements

This research has been sponsored by the Flemish Institute for the Improvement of the Scientific and Technological Research in Industry (IWT), the Fund for Scientific Research-Flanders (FWO) Belgium.

The authors also acknowledge the Flemish government (GOA-Optimech) and the research council of the Vrije Universiteit Brussel (OZR) for their funding. The first author hold a grant as a Postdoctoral Researcher from the FWO Vlaanderen.

References

[1] W. Heylen, S. Lammens, P. Sas, *Modal Analysis Theory and Testing*, PMA, KULeuven, 1998.
[2] D.J. Ewins, *Modal Testing: Theory and Practice*, Research Studies Press, Taunton, 1985.
[3] P. Castellini, G.M. Revel, L. Scalise, Measurement of vibrational modal parameters using laser pulse excitation techniques, *Measurement* 35 (2004) 163–179.
[4] B.T. Hefner, P.L. Marstona, Magnetic excitation and acoustical detection of torsional and quasi-flexural modes of spherical shells in water, *Journal of the Acoustical Society of America* 106 (1999) 3340–3347.
[5] J. Deweer, B. Dierckx, Obtaining a scaled modal model of panel type structures using acoustic excitation, *Proceedings of the XVIIth International Modal Analysis Conference*, Orlando, USA, 1999.
[6] F. Daerden, P. Guillaume, Binary sequence excitation by pressurized air, *Proceedings of the 25th International Seminar on Modal Analysis*, Leuven, Belgium, 2000.
[7] J.F. Blackburn, *Pressure-flow Characteristics of Pneumatic Valves: Fluid Power Control*, The MIT Press, Cambridge, 1960.
[8] ISO 6358, Pneumatic fluid power—components using compressible fluids—determination of flow-rate characteristics, 1989.
[9] D. Phares, G.T. Smedley, R.C. Flagan, The wall shear stress produced by the normal impingement of a jet on a flat surface, *Journal of Fluid Mechanics* 418 (2000) 351–375.
[10] K. Godfrey, *Perturbation Signals for System Identification*, Prentice-Hall, Hertfordshire, 1993.
[11] E. Parloo, P. Verboven, P. Guillaume, M. Van Overmeire, Force identification by means of in-operation modal models, *Journal of Sound and Vibration* 262 (2003) 161–173.